

SELF-ASSEMBLY OF CELLULOSE NANOCRYSTALS WITH FLUORESCENT AGENT IN IRIDESCENT FILMS

RAPHAEL BARDET,* CÉCILE SILLARD,* NACEUR BELGACEM** and JULIEN BRAS***

**Université Grenoble Alpes, LGP2, F-38000 Grenoble, France*

***CNRS, LGP2, F-38000 Grenoble, France*

****LGP2/Grenoble INP-Pagora/CNRS - 461 rue de la papeterie, Domaine universitaire, BP 65, 38402 Saint Martin d'Hères cedex, France*

✉ *Corresponding author: Julien Bras, julien.bras@grenoble-inp.fr*

Sulfated cellulose nanocrystals (CNCs) undergo self-organization in concentrated suspensions, leading to the formation of an iridescent film under specific drying conditions. In this study, CNCs were combined with the optical brightening agent (OBA), distyrylbiphenyl sulfonate (DSBP), which imparts fluorescence to the iridescent film as an additional property. The influence of DSBP on the CNC suspension is limited, thus the self-organization and the structural coloration (iridescent) of the film obtained by simple evaporation are preserved. The first section of the study outlines the influence of DSBP on the CNC suspension based on various analyses, including zeta potential measurements, dynamic light scattering (DLS), quartz crystal microbalance (QCM), and atomic force microscopy (AFM). From fluorescence spectroscopy, the amount of DSBP labeled onto the CNCs is determined to be $\sim 18 \mu\text{mol/g}$. Solid films based on DSBP-labeled CNC were also produced and characterized via UV spectroscopy. These films appear both colored in natural light, due to preservation of the self-assembly of CNC, and fluorescent under UV-illumination because of the fluorescent agent.

Keywords: nanocellulose, cellulose nanocrystals, iridescence, fluorescence, film

INTRODUCTION

The growth of globalized trading and online shopping is accompanied by attendant issues such as counterfeiting of high-value products. According to the Organization for Economic Co-operation and Development (OECD), the value of international trade with counterfeit goods has been estimated at \$500 billion, with a growth rate of 1,700% over the past 10 years.¹ In parallel, statistics published by the European Commission show that the growth in terms of volume, sophistication, and range of counterfeit goods, as well as the number of affected countries has continued to expand.² Anti-counterfeiting technology is one method used to protect both companies and customers. In general, anti-counterfeiting technologies should be easily applied, but difficult to imitate. Some anti-counterfeiting technologies are low cost and user friendly, while others are highly sophisticated and expensive. Manufacturers have several different technologies to functionalize their products or packaging with anti-counterfeiting features. These include watermarks, specialized printing, the use

of holographic labels, and the use of synthetic fibers or additives.³

The use of biomaterials for the design of photonic nanostructures is an emerging perspective in the field of optical encryption technology that was first recognized in 2010. Cellulose nanocrystals (CNCs) are one such biomaterial with the recognized property of self-assembly in a suspension; this leads to the formation of an iridescent film under specific drying conditions. These rod-like nanoparticles (about 5 nm wide and 250 nm in length), which can be extracted from vegetal biomass, feature an attractive combination of promising properties, such as being bio-based, biodegradable, and biocompatible, as well as having low density (~ 1.6), high stiffness (~ 150 GPa), high thermal stability (~ 300 °C), and possessing a high density of hydroxyl groups, making chemical modification and self-organization possible. Recent studies (later than 2010) not only describe the characterization and production of CNCs, but also increasingly frequently address their end use

in smart applications, such as for controlling drug release,⁴ as aerogels for insulation,⁵ as stimuli-responsive materials,⁶ and as photonic films.⁷ There is a growing interest at the industrial level, with the recent construction of the first CNC processing plants and the growth of the patent portfolio since the year 2008.⁸ This study focuses only on the self-organization properties of CNCs; however, more detailed information about the production, characterization, and utilization of CNCs can be found in a recent book⁹ or reviews.¹⁰⁻¹²

Revol, Godbout, and Gray¹³ presented the pioneering report that the self-organization of oriented CNC may be preserved in a film obtained under free and undisturbed evaporation. As a rule of thumb, if the pitch of solid films is approximately the wavelength of visible light, iridescent and colored films are obtained. This is the origin of the structural coloration of films based on CNC, a feature that opened the prospects for new high-value applications of nanocellulose.⁸

In parallel, several studies have investigated the grafting of fluorophore molecules onto CNCs, mainly for sensor or imaging in biomedical applications.¹⁴ This includes aminofluorescein¹⁵ (DTAF) and fluorescein isothiocyanate (FTIC),^{16,17} which was fabricated through a three-step reaction. By exploiting papermaking science, another fluorescent molecule may be labeled onto CNC. Indeed, distyrylbiphenyl sulfonate (DSBP) derivatives are widely used as efficient optical brightening agents (OBAs) to improve the brightness of paper, and these derivatives exhibit excellent affinity toward cellulose fibers.¹⁸ The combination of a CNC suspension with an OBA agent (Tinopal® HW) has recently been proposed by Zhang and coworkers,¹⁹ who reported a simple and efficient method to manufacture an iridescent film with fluorescent properties.

However, they reported a red shift in the emission of the iridescent film with increasing concentration of OBA and no evidence of the labeling with DSPB was reported. Based on these studies, we investigated the functionalization of an iridescent film with another grade of disulfonated DSPB (Tinopal® CBS), as summarized in Figure 1. In this study, commercial CNCs produced on the pilot-scale are selected for easier technology transfer. As a preliminary investigation, the labeling of DSBP is investigated based on QCM-D, zeta potential, and AFM analyses. The degree of labeling is also evaluated based on extensive purification of CNC

and fluorescence spectroscopy. Furthermore, iridescent and fluorescent films are manufactured and characterized using UV-Visible spectroscopy.

EXPERIMENTAL

Materials

The starting material for producing the iridescent solid films is commercial cellulose nanocrystals (CNC), delivered as a dry powder. CNC was purchased from Celluforce (Allure™, Canada) and isolated from wood pulp by sulfuric acid hydrolysis. The commercial fluorescent agent (Tinopal® CBS, BASF, Germany) is a 27 wt% solution of 4,4'-distyrylbiphenyl sodium sulfonate salt (DSPB) with a molar weight of 562 g/mol, used as received. Polyethylenimine (PEI) with a molecular weight of 1300 g/mol was purchased from Sigma-Aldrich (USA). Deionized water (5 µS/cm) was used in all experiments.

Methods

CNC suspension and DSBP solution preparation

After dilution to 5.0 wt%, the CNC suspension was subjected to dispersion under a force of 1 kJ/g_{CNC} using a 200 W sonication probe (Sonifier® S-250A, Branson, USA) in order to obtain a homogeneous dispersion.

A 100 µM solution (500 ml) of DSPB was prepared by diluting the commercial DSPB solution. For spectroscopic analyses, diluted solutions with concentrations ranging from 1 µM to 100 µM were also prepared. All DSBP solutions were mixed in a flask wrapped in aluminum foil to prevent photolysis of OBA.

Nanoparticle characterization

Individual nanoparticles were imaged using an Atomic Force Microscope (AFM; Nanoscope III®, Veeco, Canada). All samples were pre-diluted to 10⁻⁴ wt% and a 0.2 mL drop of the sample was deposited on freshly cleaved Mica substrates and dried overnight under room conditions. Each sample was characterized with a silicon cantilever (OTESPA®, Bruker, USA) in tapping mode at four different locations and two scanning areas: 3 x 3 µm² and 1 x 1 µm². Topographical, as well as phase images were captured, and the resulting images were subjected to 1st-order polynomial flattening to reduce the effects of bowing and tilt. Only the most representative images are presented in this study; however, the morphological dimensions were obtained as an average of at least 50 individual nanoparticles.

X-ray diffraction (XRD) patterns were acquired for the powdered CNC film using an X-ray diffractometer (PANanalytical®, X'Pert PRO MPD). The operating conditions for the refractometer were CuKα radiation (1.5418 Å), 2θ Bragg angle between 5° and 60°, step size of 0.067°, and a counting time of 90 s. The

cellulose crystallinity index (CI) was evaluated using the empirical method developed by Segal and coworkers.²⁰ For each XRD pattern, the data were acquired twice and then averaged.

The surface charge was determined via conductometric titration. 15 g of the CNC suspension (1 g dried CNC) was stirred with 250 mL of a 0.1 M HCl solution for 10 minutes. The suspension was then

extensively dialyzed (Spectra/Por® 4, SpectrumLabs, USA) against a large excess of deionized water over 7 days. Subsequently, the conductivity of the suspension was adjusted to 700 $\mu\text{S}/\text{cm}$ by addition of 0.1 M NaCl solution and then titrated with a 10 mM NaOH solution in 0.1 mL increments until all charged groups were neutralized. Each titration was performed in triplicate.

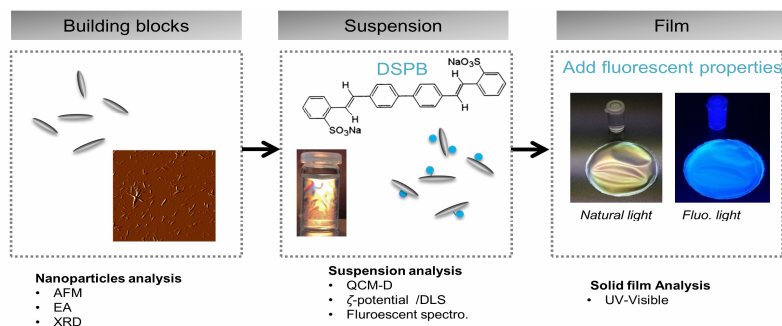


Figure 1: Graphical abstract

Chemical interactions between CNC and fluorescent agent

The electrophoretic mobility of CNC was measured using a zeta potential analyzer (Zeta2000, Malvern Instruments, USA). CNC suspensions were diluted to around 0.1 wt% in deionized water or in a 100 μM DSPB solution. NaCl solution was added to maintain the conductivity of the suspension (500 $\mu\text{S}\cdot\text{cm}^{-1}$). The electrophoretic mobility (μ_e and zeta potential) reported herein is an average of 10 measurements.

Dynamic light scattering (DLS) was used to measure the size of the nanoparticles (Vasco® I, Corduan Technologies, France). All the samples were previously diluted in DI water to a concentration of 10⁻² wt%, and the conductivity was adjusted to 500 $\mu\text{S}/\text{cm}$ by addition of NaCl solution. The cumulative method was used and two parameters were taken into account, i.e. the hydrodynamic diameter (z^*) and the polydispersity index (*PDI*). For each sample, 10 acquisitions were performed and each measurement was replicated 3 times.

Adsorption measurements were performed with a Quartz Crystal Microbalance with Dissipation (QCM-D). The instrument (Q-Sense® E1, Biolin Scientific, Sweden) measures the resonance frequency of the oscillation of a quartz crystal based on the fundamental frequency (5 MHz) and selected overtones (15, 25, 35, 45, 55, and 75 MHz). Only the seventh overtone is used in the data evaluation. The adsorbed mass (ng/nm^2) was estimated from the frequency change (Δf) using Sauerbrey's equation. Sorption curves were acquired using 100 nm gold-coated quartz crystals (QSX301, Biolin Scientific, Sweden). All

measurements were performed under constant flow rate (100 $\mu\text{L}/\text{min}$) and temperature (23 °C).

Prior to the analyses, the gold surfaces were cleaned by immersion in a "piranha" solution (30% of H₂O₂/NH₃, 1:3 by weight) for 20 minutes at 70 °C, then rinsed with deionized water and finally subjected to UV/ozone treatment (ProCleaner™, Bioforce, USA) for 20 minutes. Prior to the analysis, a 100 μM cationic polyethylenimine solution (PEI, Sigma Aldrich) was first adsorbed onto the cleaned gold surfaces to facilitate CNC adsorption, as well as their irreversible bonding with the crystal sensor. At the beginning of each experiment, deionized water was passed through the chamber until a stable baseline ($\Delta f < 0.05/\text{min}$) was achieved (5-20 minutes).

Fluolabeled CNC solution

To achieve a final concentration of 20 $\mu\text{mol}/\text{g}$ of DSPB, 0.5 wt% CNC suspension was mixed with a 100 μM DSPB solution and stirred for 20 min at a constant stirring rate. The fluorescent CNC suspension was then purified by prolonged dialysis (Spectra/Por®4, SpectrumLabs, USA) against a large excess of deionized water (in the dark) until the presence of DSPB in the external dialysis reservoir could not be detected (7 days).

Degree of labeling

The amount of DSPB labeled onto the CNCs was assessed using fluorescence spectroscopy (LS 50B, Perkin-Elmer, USA) at 20 °C. The DSPB content of the labeled CNC samples was determined from calibration curves previously established using DSPB

standards (0-100 μM range). Fluorescence scans were obtained using the following settings (optimized for a 100 μM DSBP solution): 4 nm slit widths, 350 nm excitation, emission scanned from 360 to 600 nm. Three independent measurements were obtained for each sample.

Solid film formation

Approximately 34 mL of the various 0.5 wt% CNC suspensions (with or without DSPB, before or after dialysis) was casted on a smooth aluminum plate (6 cm diameter) and left to dry for 3 days under room conditions (50% RH, 23 °C). For each series, 4 dried free-standing films of 60 g/m^2 were thus obtained and stored under these conditions until analysis.

Film characterization

The structurally colored films were analyzed using UV-Visible spectroscopy (UV 1800, Shimadzu, Japan). The absorption intensity of the solid film was recorded within the wavelength range of 200 to 1100 nm with a normal incidence. For each sample, three independent measurements and ten scans were recorded and averaged. For observation under UV illuminant ($\lambda=365$ nm), a UV lamp (VL 215G, Bioblock Scientific, France) was used.

RESULTS AND DISCUSSION

Nanocellulose characterization and photophysical properties of DSBP

Prior to film formation, the physical and chemical properties of the commercial cellulose nanocrystal (CNC) suspension were determined. As presented in Figure 2-A, the CNCs had an elongated, rod-like morphology with average dimensions of 8 nm thickness by 174 nm length.

This morphology of the nanoparticles is in accordance with previous studies of CNCs extracted under similar hydrolysis conditions (wood pulp, sulfuric acid). The XRD pattern (not

presented) is typical of the crystalline polymorph of neat cellulose I (native cellulose). The major crystalline peak (002) occurs at 22.84° and the associated crystallinity index (CI) is 88%. The surface charge, associated with the content of sulfate ester groups, is about 190 $\mu\text{mol}/\text{g}$ (estimated by conductometric titrations). Based on the surface charge estimation and the geometric dimensions of the CNCs derived from the AFM images, the surface charge density is about 0.38 e/nm^2 . As a comparison, surface charge densities of 0.16 to 0.64 e/nm^2 were reported in self-assembly studies of CNC suspensions.⁹ The 0.5 wt% CNC suspension dispersed in water displays intense birefringence patterns (Figure 2-B). This confirms the absence of agglomeration as well as preservation of the self-assembly properties of CNC in suspension. Thus, it is demonstrated that the CNCs are well isolated from cellulosic fibers; they have a rod-like morphology, and display self-assembly properties in water.

The photo-physical parameters of the distyrylbiphenyl sodium sulfonate (DSBP) salt used as the fluorescent agent were also investigated. Figure 3-A shows that DSBP absorbs in the UV spectral range ($\lambda_{\text{abs}} = 351$ nm) and emits strong blue fluorescence ($\lambda_{\text{em}} = 425$ nm). Such spectral features are in agreement with those reported in other previous studies.¹⁹

A calibration curve (Figure 3-B) (normalized fluorescence intensity as a function of the DSBP dosage) was constructed to determine the amount of DSBP labels attached to the CNCs. Good correlation between the fluorescence intensity and DSPB concentration was observed between 0 to 100 μM .

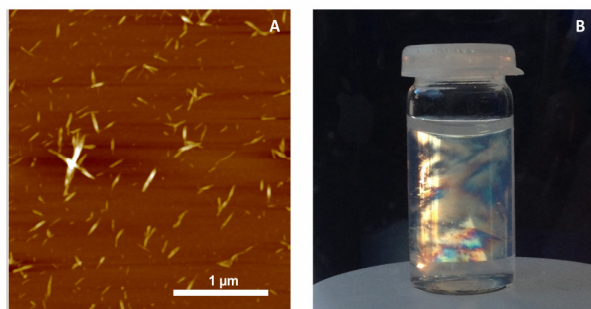


Figure 2: Observation of a 0.5 wt% CNC suspension between cross-polarizers (A) and AFM image showing individualized CNCs (B)

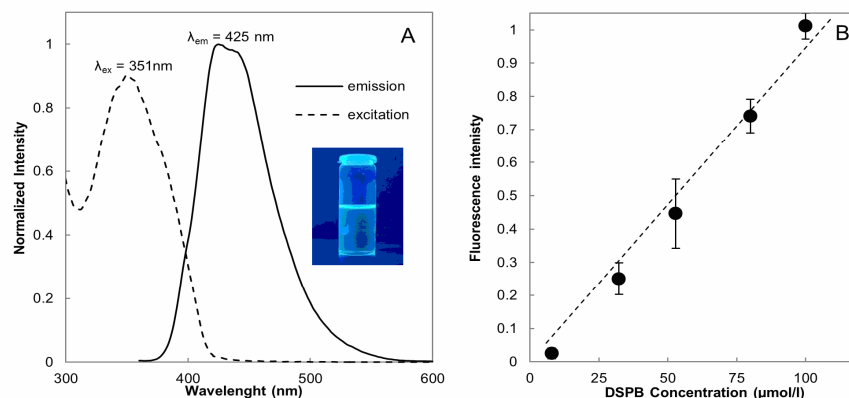


Figure 3: Fluorescence spectra of 100 μM DSBP solution (A) and calibration curve of DSBP solution (B); (Calibration curve was obtained from 1 μM to 100 μM using an excitation wavelength of 351 nm; intensities reported in fluorescence spectra and calibration curves were standardized from 100 μM DSBP solutions)

Table 1
Electrokinetic potential, hydrodynamic size, and colloidal behavior of 0.5% CNC suspension dispersed in water and in 100 μM water-soluble polymer solutions

CNC dispersion (0.5 wt%)	Hydrodynamic properties ^a		Electrokinetic potential ^b		Colloidal behavior ^c
	z^* (nm)	PDI	$p\zeta$ (mV)	Ue (V)	
Deionized water	105 (5)	0.2	-44.8 (1.2)	-3.5 (0.07)	Birefringent
In DSBP solution (100 μM)	105 (10)	0.18	-50.8 (0.8)	-3.82 (0.08)	Birefringent
PEI polymer solution (100 μM)	856 (8)	0.75	15 (1.1)	1.18 (0.09)	no

Note: Measured by DLS^a and Zeta potential^b analyses; Observation between cross-polar after stirring^c; Values in brackets indicate standard deviation

Interactions between CNC particles and DSBP solution

Prior to fabricating the fluorescent and iridescent CNC films, the influence of adding anionic DSBP to the CNC suspension was evaluated. This is a critical point given that the self-organization of CNCs is sensitive to the electrochemical equilibrium.²¹⁻²³ Moreover, the addition of water soluble molecules (monovalent salt,²⁴ cationic polymers,²⁵ or surfactants)²⁶⁻²⁷ can completely modify the CNC self-assembly properties.

The ζ -potential is used to quantify the electrostatic repulsive forces and gives an indication of the potential stability of the colloidal system and indirectly of their self-organization. A value lower than ± 15 mV is considered as the onset of particle agglomeration. Values higher than ± 30 mV generally mean that there is sufficient mutual repulsion, which ensures the colloidal stability.²⁸

Table 1 compares the hydrodynamic and electrokinetic parameters of CNC suspended in deionized water with those containing anionic

additives. The zeta potential of CNC dispersed in deionized water is highly negative (-45 mV) due to the high surface charge density of the sulfate half-ester groups.²⁴ In the presence of anionic DSBP, the mobility remains highly negative and the hydrodynamic diameter is unmodified. Consistent with a previous similar study,¹⁹ an increase (-51 mV) of the zeta potential was observed when CNC was suspended in DSBP solution, which can be attributed to sorption of DSBP on the hydroxyl surface groups. The suspension in DSBP solution displays birefringence patterns owing to preservation of the self-organization imparted by the highly negative surface charges of CNC.

In contrast, in the case of dispersion in 100 μM PEI solution, the flow birefringence disappears and the zeta potential is shifted from -44.5 mV to +15.0 mV. This confirms ionic bonding between the negative sulfated groups of CNC and amino groups of this polymer. This interaction also leads to particle flocculation ($z^* = 856$ nm), as detected via DLS measurement. The last experiment was conducted in order to

evaluate the adsorption phenomena associated with the PEI solutions used for functionalization of the gold-coated mica plate for QCM experiments.

Sorption phenomena of DSPB with CNC

Adsorption measurements were performed with a quartz crystal microbalance with dissipation (QCM-D), as shown in Figure 4.

As a preliminary investigation, the thickness of the adsorbed CNC layer was analyzed to determine if the layer was sufficiently thick to prevent interaction of the positively charged substrate with PEI. Based on the frequency drop ($\Delta f = -62 \pm 2$ Hz) and deduction using Sauerbey's equation, the average weight of CNC adsorbed on the substrate is 1.1 g/m^2 . This corresponds to a CNC layer of about 8 nm assuming that the density of the CNC layer is 1.44. Thus, the adsorbed CNC layer is sufficiently thick to prevent artifact sorption with the charged substrate (PEI layer). The amount of adsorbed

CNC is similar to that reported (c.a. 10 nm) under equivalent experimental conditions.²⁹

AFM analyses were also carried out on the air-dried substrate surface after CNC adsorption and rinsing with DI water (Figure 5-A). Notably, the adsorbed CNC layer displays good surface coverage with random orientation of the rods. Moreover, the CNC layer formed a three-dimensional network with a large exposed surface area. Instead of uniform adsorption of water-soluble polymers to form a smooth layer, the adsorbed CNC layer formed a non-continuous layer (

Figure 5-A).

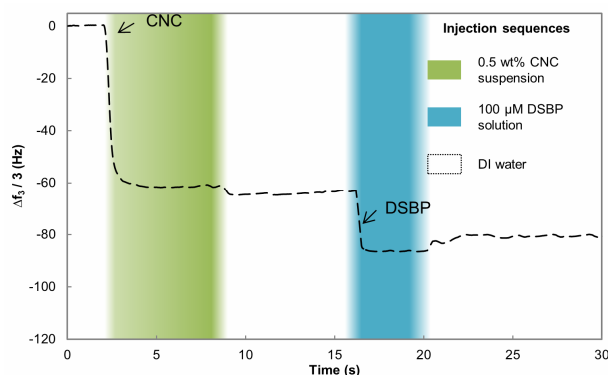


Figure 4: QCM-D study (3rd overtone) of CNC and DSPB adsorption on PEI modified gold surface; (The 1st injection corresponds to 0.5 wt% CNC suspension (green area), the 2nd injection to the injection of 100 μM DSPB solution (blue area), uncolored sections correspond to the rinsing stage with DI water; $\Delta f_3/3$ - the frequency drop normalized by the overtone, is a measure of the absorbed mass including bound water)

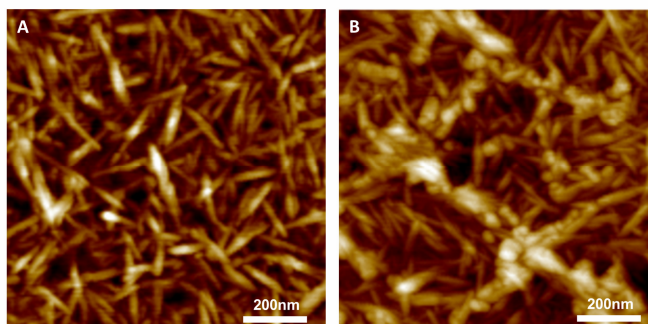


Figure 5: AFM pictures (height sensor) corresponding to air-dried substrate analysis during QCM experiments - after injection of CNC and rinsing (A), after injection of DSPB and rinsing (B)

Consequently, in calculating the mass of DSPB adsorbed on the CNCs, the specific surface topography of the CNC layer must be taken into consideration.³⁰ From a calculation carried out for three 9 μm^2 scanning areas, the surface formed by the CNC layer is estimated to be $16 \pm 2 \mu\text{m}^2$. This means that a surface area of 1.8 cm^2 should be considered for 1 cm^2 of the surface sensor. Moreover, based on the heterogeneity of the CNC substrate, the amount of polymer adsorbed should be considered semi-quantitative.

With the addition of DSPB, there is a frequency drop ($\Delta f = -62 \pm 2 \text{ Hz}$) (Figure 4), suggesting the adsorption of anionic DSPB molecules onto CNC. The nonionic interactions between the additive and the cellulose surface lower the repulsive barrier towards the polyelectrolyte, facilitating adsorption on the CNC surface. Similar to cellulosic fibers, the physical adsorption of DSPB is primarily related to the electrostatic interaction with the surface via the sulfonic groups of DSPB and formation of strong hydrogen bonds.³¹ Additionally, after injection of DSPB, moderate desorption ($\Delta f \sim +7 \text{ Hz}$) was also observed during rinsing with DI water. Nevertheless, the mass of DSPB adsorbed on CNC remained significant ($\Delta f \sim 21 \text{ Hz}$, i.e. 360 ng/cm^2). The AFM image (Figure 5-B) of DSPB adsorbed on CNC suggests that DSPB is not uniformly distributed on the CNC surface. Clustered spherical particles fixed on CNC may

undergo agglomeration. Similar aggregation was reported for macroscopic fibers.³²

Considering a CNC surface area³³ of about 150 g/m^2 and the “real” surface area of the CNC layer, the adsorption of DSPB is estimated to be $53 \pm 11 \mu\text{mol}/\text{g}$.

Efficiency of DSPB sorption on CNCs

The affinity of DSPB for the CNCs was evaluated from zeta potential, DLS, and QCM analyses. DSPB could be labeled onto the CNCs at a loading (adsorbed amount) of about 50 $\mu\text{mol}/\text{g}_{\text{CNC}}$.

To confirm the degree of labeling, a 0.5% CNC suspension was mixed with a 100 μM DSPB solution (i.e. 50 $\mu\text{mol}/\text{g}_{\text{CNC}}$). The CNC and DSPB mixture was sonicated and purified by prolonged dialysis (7 days) to remove the unadsorbed fluorescent agent (Figure 6). Dialysis was discontinued when fluorescence of DSPB could no longer be detected in the contents of the external dialysis reservoir. In parallel, a control solution (without CNC) was also purified (Figure 6-D and E). The fluorescence spectra of the samples were recorded (Figure 6) to determine the degree of labeling using the calibration curve (Figure 3).

As expected, the neat CNC suspension was non-fluorescent (Figure 6-A), whereas CNC suspensions containing DSPB before and after dialysis (Figure 6-B and C) emitted strong fluorescence ($\lambda_{\text{em}} = 425 \text{ nm}$).

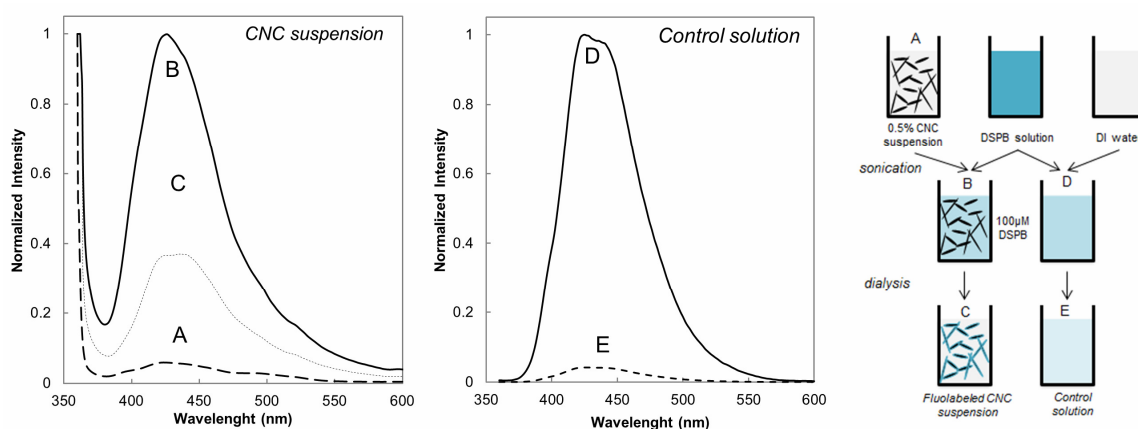


Figure 6: Fluorescence spectra of 0.5 wt% neat CNC suspension (A), with 100 μM DSPB solution before (B) and after dialysis (C); control spectra corresponding to the 100 μM DSPB solution before (D) and after dialysis (E); (Intensities are standardized with respect to the absorbance of a 100 μM DSPB solution, $\lambda_{\text{ex}} = 351 \text{ nm}$)

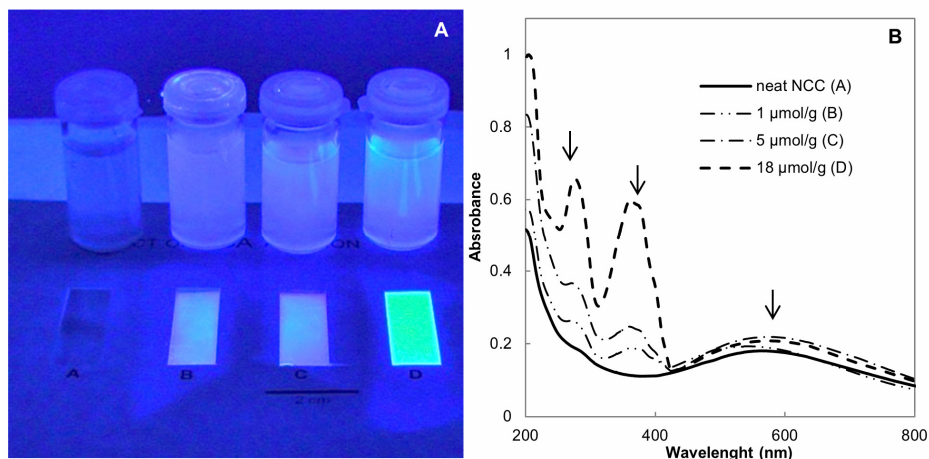


Figure 7: Observation of CNC suspensions and 60 g/m² solid films with increasing amount of DSPB (0 to 11 µmol/g) under UV illuminant ($\lambda=365$ nm) (A), and corresponding UV-visible spectra (B)

The removal of DSPB molecules from dialyzed CNC was indicated by a decrease in the fluorescence intensity, corresponding to a decrease in the DSPB concentration. From the calibration curve, the amount of DSPB labeled onto CNC is estimated to be 38 ± 3 µM, i.e. 19 µmol/g_{CNC}. For the control solution (100 µM DSPB solution without CNC), the absence of a DSPB adsorption peak indicates that almost all of the DSPB in the DI water was removed after

As a comparison, a value twenty times lower (1 µmol/g) was reported for DSPB adsorbed on cellulosic fibers.³⁴ Such a difference may be related to the difference between the surface area of the cellulosic fibers³⁵ and CNCs³³ of 1-3 m²/g and 150 m²/g, respectively.

Compared with fluorescent molecules grafted onto CNCs, the amount of DSPB is equivalent to fluorescein isothiocyanate¹⁶⁻¹⁷ (FTIC) with values ranging from 3 to 30 µmol/g and several times higher (5-50 nmol/g) than that of grafted aminofluorescein¹⁵ (DTAF).

Another point of interest in using DSPB instead of other fluorescent molecules is that the labeling could be carried out without chemical modification and did not require the use of a multistep reaction.

Formation of fluorescent and iridescent film based on CNCs

To prepare 60 g/m² iridescent films with varying amounts of DSPB, the fluolabeled CNC suspension was mixed with neat CNC suspensions. The incorporation of fluorescence properties into the iridescent film may be promising for improving optical encryption of

purification. It should be noted that the amount of DSPB labeled onto the CNCs reported herein (19 µmol/g_{CNC}) is even lower than the value calculated from QCM (53 µmol/g_{CNC}). This may be due to the assumptions made for the calculation based on QCM experiments, such as the surface area of CNC or the surface topography of the CNC layer. This discrepancy may also be related to the measurement time being too brief during the desorption cycle (only 10 minutes). solid films.¹⁹ The ratio of DSPB ranged from 0 µmol/g of DSPB (100% of neat CNC suspension) to 18 µmol/g (100% of fluolabeled CNC suspension).

Figure 7 shows moderate fluorescence for the samples containing 1-5 µmol/g of CNC, whereas more intense fluorescence was achieved when more DSPB was used (18 µmol/g). In addition, the coloration under natural light was preserved with a slight red shift from 546 nm to 578 nm of λ_{max} in the visible spectra. The absorption peak observed at 367 nm corresponds to the maximal excitation wavelength of DSPB, the intensity of which increased with the amount of adsorbed DSPB. The prepared films appear colored under natural illumination due to preservation of the self-organized structure of CNC and are fluorescent under UV illumination because of the fluorescent agent.

CONCLUSION

The adsorption of the anionic fluorescent agent DSPB onto CNCs was confirmed by QCM analyses. Adsorption occurs via electrostatic interaction of the sulfonic groups of DSPB and formation of strong hydrogen bonds with the

CNCs. The amount of DSPB adsorbed on the CNCs is about 18 $\mu\text{mol/g}$ based on fluorescence spectroscopy. This limited interaction of DSPB with the CNC suspension preserves the self-assembly of the CNC suspension and the structural coloration (iridescent) of the film obtained by simple evaporation. The combination of CNC with the optical brightening agent, distyrylbiphenyl sulphonate, imparts fluorescence to the iridescent film as an additional property. The prepared films appear colored in natural light because of the preservation of the self-organization of CNC and fluorescent under UV-illumination because of the fluorescent agent.

REFERENCES

- ¹ T. Staake, F. Thiesse and E. Fleisch, *Eur. J. Marketing*, **43**, 320 (2009).
- ² J. Spink, D. C. Moyer, H. Park and J. A. Heinonen, *Crime Sci.*, **2**, 1 (2013).
- ³ L. Li, *Business Horizons*, **56**, 167 (2013).
- ⁴ J. K. Jackson, K. Letchford, B. Z. Wasserman, L. Ye, W. Y. Hamad, *et al.*, *Int. J. Nanomed.*, **6**, 321 (2011).
- ⁵ L. Heath and W. Thielemans, *Green Chem.*, **12**, 1448 (2010).
- ⁶ J. Mendez, P. K. Annamalai, S. J. Eichhorn, R. Rusli, S. J. Rowan *et al.*, *Macromolecules*, **44**, 6827 (2011).
- ⁷ K. E. Shopsowitz, W. Y. Hamad and M. J. MacLachlan, *J. Am. Chem. Soc.*, **134**, 867 (2011).
- ⁸ H. Charreau, M. Foresti and A. Vazquez, *Recent Pat. Nanotechnol.*, **7**, 56 (2013).
- ⁹ A. Dufresne, "Nanocellulose, From Nature to High Performance Tailored Materials", De Gruyter, Berlin, 2012.
- ¹⁰ R. J. Moon, A. Martini, J. Nairn, J. Simonsen and J. Youngblood, *Chem. Soc. Rev.*, **40**, 3941 (2011).
- ¹¹ Y. Habibi, L. A. Lucia and O. J. Rojas, *Chem. Rev.*, **110**, 3479 (2010).
- ¹² S. J. Eichhorn, A. Dufresne, M. Aranguren, N. E. Marcovich, J. R. Capadona *et al.*, *J. Mater. Sci.*, **45**, 1 (2010).
- ¹³ J.-F. Revol, L. Godbout and D. Gray, *J. Pulp Pap. Sci.*, **24**, 146 (1998).
- ¹⁴ J. V. Edwards, N. T. Prevost, A. D. French, M. C. Concha, A. Delucca *et al.*, *Engineering*, **5**, 20 (2013).
- ¹⁵ T. Abitbol, A. Palermo, J. M. Moran-Mirabal and E. D. Cranston, *Biomacromolecules*, **14**, 3278 (2013).
- ¹⁶ S. Dong and M. Roman, *J. Am. Chem. Soc.*, **129**, 13810 (2007).
- ¹⁷ L. J. Nielsen, S. Eyley, W. Thielemans and J. W. Aylott, *Chem. Commun.*, **46**, 8929 (2010).
- ¹⁸ H. Zhang, Z. He, Y. Ni, H. Hu and Y. Zhou, *Pulp Pap. - Can.*, **110**, 20 (2009).
- ¹⁹ Y. P. Zhang, V. P. Chodavarapu, A. G. Kirk and M. P. Andrews, *Organic Photonic Materials and Devices XIV*, **8258**, (2012).
- ²⁰ L. Segal, J. J. Creely, A. E. Martin Jr. and C. M. Conrad, *Text. Res. J.*, **29**, 786 (1959).
- ²¹ J. Araki, M. Wada and S. Kuga, *Langmuir*, **17**, 21 (2000).
- ²² M. M. de Souza Lima and R. Borsali, *Macromol. Rapid Commun.*, **25**, 771 (2004).
- ²³ J. Pan, W. Hamad and S. K. Straus, *Macromolecules*, **43**, 3851 (2010).
- ²⁴ X. M. Dong and D. G. Gray, *Langmuir*, **13**, 2404 (1997).
- ²⁵ C. C. Y. Cheung, M. Giese, J. A. Kelly, W. Y. Hamad and M. J. MacLachlan, *ACS Macro Lett.*, **2**, 1016 (2013).
- ²⁶ S. Elazzouzi-Hafraoui, J.-L. Putaux and L. Heux, *J. Phys. Chem. B*, **113**, 11069 (2009).
- ²⁷ J. A. Kelly, K. E. Shopsowitz, J. M. Ahn, W. Y. Hamad and M. J. MacLachlan, *Langmuir*, **28**, 17256 (2012).
- ²⁸ H. Mirhosseini, C. P. Tan, N. S. A. Hamid and S. Yusof, *Colloid. Surface. A*, **315**, 47 (2008).
- ²⁹ S. Ahola, X. Turon, M. Osterberg, J. Laine and O. Rojas, *Langmuir*, **24**, 11592 (2008).
- ³⁰ S. Ahola, M. Österberg and J. Laine, *Cellulose*, **15**, 303 (2008).
- ³¹ E. T. Iamazaki and T. D. Z. Atvars, *Langmuir*, **23**, 12886 (2007).
- ³² E. T. Iamazaki, M. A. Pereira-Da-Silva, A. J. F. Carvalho, R. B. Romero, M. C. Gonçalves *et al.*, *J. Appl. Polym. Sci.*, **118**, 2321 (2010).
- ³³ P. Terech, L. Chazeau and J. Y. Cavaille, *Macromolecules*, **32**, 1872 (1999).
- ³⁴ E. T. Iamazaki and T. D. Z. Atvars, *Langmuir*, **22**, 9866 (2006).
- ³⁵ W. E. Scott, "Principles of Wet End Chemistry", Tappi Press, Atlanta, 1996.